

1 **Observed response of stratospheric and mesospheric composition to sudden**
2 **stratospheric warmings.**

3
4 *M. H. Denton^{1,2}, R. Kivi³, T. Ulich⁴, C. J. Rodger⁵, M. A. Clilverd⁶,*
5 *J. S. Denton⁷, and M. Lester⁸.*

6
7
8 1. Center for Space Plasma Physics, Space Science Institute, CO 80301, USA.

9 2. New Mexico Consortium, Los Alamos, NM 87544, USA.

10 3. Space and Earth Observation Centre, Finnish Meteorological Institute, Sodankylä, Finland.

11 4. Sodankylä Geophysical Observatory, Sodankylä, Finland.

12 5. Department of Physics, University of Otago, Dunedin, New Zealand.

13 6. British Antarctic Survey (NERC), Cambridge, UK.

14 7. Nuclear and Radiochemistry (C-NR), Los Alamos National Laboratory, Los Alamos, USA.

15 8. Department of Physics and Astronomy, University of Leicester, Leicester, UK.
16

17 **ABSTRACT:** In this study we investigate and quantify the statistical changes that occur in the
18 stratosphere and mesosphere during 37 sudden stratospheric warming (SSW) events from 1989 to
19 2016. We consider changes in the in-situ ozonesonde observations of the stratosphere from four
20 sites in the northern hemisphere (Ny-Ålesund, Sodankylä, Lerwick, and Boulder). These data are
21 supported by Aura/MLS satellite observations of the ozone volumetric mixing ratio above each site,
22 and also ground-based total-column O₃ and NO₂, and mesospheric wind measurements, measured
23 at the Sodankylä site. Due to the long-time periods under consideration (weeks/months) we
24 evaluate the observations explicitly in relation to the annual mean of each data set. Following the
25 onset of SSWs we observe an increase in temperature above the mean (for sites usually within the
26 polar vortex) that persists for >~40 days. During this time the stratospheric and mesospheric ozone
27 (volume mixing ratio and partial pressure) increases by ~20% as observed by both ozonesonde and
28 satellite instrumentation. Ground-based observations from Sodankylä demonstrate the total column
29 NO₂ does not change significantly during SSWs, remaining close to the annual mean. The zonal
30 wind direction in the mesosphere at Sodankylä shows a clear reversal close to SSW onset. Our
31 results have broad implications for understanding the statistical variability of atmospheric changes
32 occurring due to SSWs and provides quantification of such changes for comparison with modelling
33 studies.

34

35

36 1. Introduction

37 The phenomenon of a Sudden Stratospheric Warming (SSW) was first identified by *Scherhag*
38 [1952] using radiosonde observations of the stratospheric temperature above Berlin. *Scherhag*
39 clearly demonstrated that the temperature of (usually cold) stratospheric air underwent an
40 extremely rapid increase ($\sim 50^{\circ}\text{C}$) in January and February of 1952. Such "*explosive warmings in*
41 *the stratosphere*" were originally termed the "*Berlin Phenomenon*" [*Scherhag*, 1952]. In
42 subsequent studies the broad physical and chemical mechanisms that underpin SSWs were revealed
43 (e.g. *Perry* [1967], *Matsuno* [1971], *Trenberth* [1973], *Schoeberl* [1978]; *Dütsch and Braun* [1980],
44 *Schoeberl and Hartmann* [1991]). In brief, planetary-scale waves from the troposphere carry
45 momentum and energy upwards into the stratosphere and mesosphere. The breaking of these
46 waves in the upper-stratosphere/mesosphere can cause the disruption and/or break-up of the polar
47 vortex (PV) [*Matsuno*, 1971]. The PV usually carries colder air from the mesosphere down into the
48 stratosphere during the polar winter. Odd-nitrogen species (NO_x) from the mesosphere are also
49 transported downward from the mesosphere in the PV. NO_x -species are long-lived during darkness
50 and chemical reactions with NO_x constitute the major loss mechanism for stratospheric ozone (O_3)
51 during the polar winter [*Brasseur and Solomon*, 1986]. Details of the chemical and dynamical
52 variation of ozone in the Arctic wintertime have since been outlined in detail (see *Tegtmeier et al.*
53 [2008a] and references therein). In contrast, the main source of O_3 is the Brewer-Dobson
54 circulation [*Dobson et al.*, 1929; *Brewer*, 1949; *Dobson* 1956] (see also *Solomon* [1999] and
55 *Butchart* [2014] and references therein). The planetary wave-breaking that accompanies the onset
56 of a SSW transports heat from lower latitudes and accelerates the Brewer-Dobson circulation
57 [*McIntyre*, 1982]. This leads to a rapid warming of the stratosphere from its previous low-
58 temperature state. Additionally the downwards transport of NO_x is also terminated, leading to a
59 cessation of O_3 losses through chemical reactions with NO_x , while the primary source of O_3 is
60 largely unchanged. In combination, these processes usually lead to a rapid increase in O_3 levels in

61 the upper stratosphere and mesosphere immediately following a SSW, with the altitudinal
62 dependence of O₃ behaviour during SSWs strongly dependent on altitude (cf. *de la Cámara et al.*
63 [2018a]).

64

65 Although SSWs have been observed in both northern and southern latitudes, they are
66 predominantly a northern hemisphere phenomenon since planetary waves in the southern
67 hemisphere usually have a much lower wave-amplitude. The literature contains a large number of
68 recent studies where the various effects of SSWs in the stratosphere and mesosphere have been
69 investigated, both observationally and theoretically (e.g. *Sofieva et al.* [2012], *Scheiben et al.*
70 [2012], *Kuttippurath and Kikulin* [2012], *Päivärinta et al.* [2013], *Damiani et al.* [2014]; *Shepherd*
71 *et al.* [2014], *Lukianova et al.* [2015], *Manney et al.* [2015], *Strahan et al.* [2016], *Meraner and*
72 *Schmidt* [2016], *Butler et al.* [2015; 2017], *Solomonov et al.* [2017]; *de la Cámara et al.* [2018a;
73 2018b]; *Smith-Johnsen et al.* [2018]). The main processes occurring in the atmosphere before and
74 after SSWs have been determined extensively in the literature and are summarized graphically in
75 Figure 1.

76

77 SSWs have received increasing attention within the community in recent years. This is
78 predominantly due to the connections between SSWs, tropospheric weather, and surface climate in
79 the northern hemisphere (e.g. *Kretschmer, et al.* [2018], and references therein). Determining the
80 occurrence date of a SSW allows forecasters to predict likely weather patterns much further in
81 advance [*Tripathi et al.*, 2015; *Pedatella et al.*, 2018]. Additionally, since the effects of SSWs
82 propagate upwards in altitude, as well as downwards, determining their morphology assists in
83 understanding topics as diverse as electron densities in the ionosphere (e.g. *Chau et al.* [2012]) and
84 satellite drag (e.g. *Yamazaki et al.* [2015]). As with many other dynamic terrestrial phenomena, the
85 classification of SSWs has proven somewhat difficult to formalize with different definitions of the

86 various types of SSW having been identified in the literature. The recent works of *Butler et al.*
87 [2015] and *Palmeiro et al.* [2015] assess the various criteria being used to identify and classify
88 SSWs and provide the impetus for more-rigid definitions throughout the community.

89
90 Despite the large number of studies of individual SSWs in the literature, there have been few
91 investigations that quantify the statistical variability in composition that occur before during, and
92 after these events (cf. *Strahan et al.* [2016]). Each event is certainly different, with different initial
93 conditions in the atmosphere, different driving mechanisms, and differing durations. Modelling
94 studies are used increasingly to provide predictions of changes in the atmosphere during SSWs, and
95 to subsequently derive the physical and chemical basis for these changes. However, such models
96 require observational data for comparison. The over-arching aim of the current study is to quantify
97 the changes that occur in the stratosphere and mesosphere regions of the atmosphere during SSWs,
98 in a statistical manner, and hence reveal the variability of atmospheric effects caused by these
99 events. Previous analyses have generally considered the effects of single SSWs during a particular
100 year. Such studies usually consider the time-series of the parameter under consideration (e.g. how
101 O₃ at a particular location changes in time). However, the observed changes during such events
102 (which may last days, weeks, or even months), are usually provided in addition to the natural
103 variation of the parameter (that would be expected to take place whether a SSW occurred or not).
104 In contrast to such analyses, the work in this study is intended to reveal (and quantify) the statistical
105 changes that occur, on average during SSWs, with respect to the underlying (naturally occurring)
106 annual variation (see also *Päivärinta et al.* [2013]; *Ageyeva et al.* [2017]). Such *seasonal-*
107 *corrections* to the data (to ascertain the deviation from the natural variation) were previously made
108 with respect to changes in O₃ during solar-proton events (SPEs) [cf. *Denton et al.*, 2017; 2018] and
109 the same techniques are used in the current study.

110

111 The data and analysis techniques used in this study are summarized in Section 2. Results are
112 presented in Section 3 and discussed in detail in Section 4. A summary of the main findings and
113 the conclusions to be drawn from this study are to be found in Section 5.

114

115 **2. Data and Analysis**

116 The study of *Bulter et al.* [2015] correctly points out that the definitions of SSWs have changed
117 over time and that a single definition to fit all users would likely be impossible. They also wisely
118 notes: "...*history suggests that a true standard definition of SSWs is at best ambiguous and at worst*
119 *nonexistent*". The problem with standards is that there are so many of them. The analyses
120 undertaken in this study concern 37 SSWs occurring between 1989 and 2016. These events are a
121 combination of the previously published events identified in Table 2 of *Butler et al.* [2017] and
122 Table 4.1 in *Ehrmann* [2012] with the events after 2013 taken from the recent literature. Here we
123 follow *Butler et al.* [2017] with SSWs defined as when the daily-mean zonal-mean zonal winds at
124 10 hPa and 60° N first change from westerly to easterly between November and March. The winds
125 must return to westerly for twenty days between events.. Table 1 contains the onset timing of the
126 events used (further details of the events can be found in *Butler et al.* [2017] and *Ehrmann* [2012]).
127 A caveat to statistical analysis of SSWs is that in each year there may be a single warming, or
128 multiple warmings (denoted in the literature as "*first warming*", "*major warming*", "*final warming*",
129 etc.). The durations, and indeed the actual definitions, of each of these (e.g. "*displacement events*",
130 "*split events*") is highly variable throughout the literature (see *Butler et al.* [2015] and *Palmeiro et*
131 *al.* [2015] for a detailed discussion of SSW definitions). The atmosphere will clearly be in a
132 somewhat different and unique state for the first warming, compared to the final warming, with
133 each event having a different time-history. However, there are certainly similarities between all
134 events particularly since the onset of a SSW occurs due to the break-up/disruption of the PV, driven
135 by breaking of planetary waves. It is these similarities that are investigated here. Separating out

136 the statistical effects of multiple warmings during a single year is not possible due to the limited
137 number of events and is beyond the scope of the current study. The main goal in the current study
138 is to quantify the mean changes taking place in stratospheric and mesospheric O₃ during a typical
139 SSW (with other parameters also being investigated). We do not aim to investigate the differences
140 between individual events but rather concentrate on the mean perturbations to be expected during
141 an "average" SSW onset. Since each event is different the most appropriate methodology to use is
142 superposed-epoch analysis (sometimes known as composite analysis). This analysis is based on
143 ordering the data from each event based on an "epoch time", here identified as the time of SSW
144 onset (from Table 1). The mean variation of each parameter with relation to the epoch time can
145 then be determined (along with percentiles, standard-deviation, etc.). This methodology was
146 previously used in the studies of ozone changes during SPEs [Denton *et al.*, 2017; 2018] as well as
147 other phenomena relating to particle precipitation into the atmosphere and subsequent changes in
148 atmospheric chemistry (e.g. Kavanagh *et al.* [2012], Denton and Borovsky [2012], Blum *et al.*
149 [2015]).

150

151 The data sets to be analyzed via superposed-epoch analysis relate to the abundance of O₃ in the
152 stratosphere and mesosphere. In addition, we also examine other selected parameters that are
153 known to affect the production, loss, and transport of ozone in the atmosphere. These include the
154 variations in stratospheric and mesospheric NO₂ (due to its link to the loss of O₃), the speed and
155 direction of the prevailing atmospheric winds (due to its role in the transport of O₃), and the
156 temperature (due to linkages with both the source and the loss processes connected with O₃). The
157 data sets associated with these variables are described in Sections 2.1-2.4 below.

158

159 **2.1 ECC ozonesonde data**

160 Frequent high-resolution ozonesonde observations are made at dozens of sites around the globe.

161 Many utilize balloon-borne Electrochemical Concentration Cell (ECC) detectors to provide the
162 ozonesonde partial pressure and temperature as a function of pressure (and geopotential altitude)
163 from the ground up to ~38 km altitude [*Deshler et al.*, 2008; 2017, *Kivi et al.*, 2007, *Smit and*
164 *ASOPOS Panel*, 2014]. The wind direction and speed can also be sampled and recorded. Here,
165 data from ECC ozonesondes launched from four sites are utilized: Ny-Ålesund on the Svalbard
166 archipelago (NY-ÅL); Sodankylä in northern Finland (SOD); (C) Lerwick on the UK Shetland
167 Isles (LER); (D) Boulder in the continental USA (BOU). The observations provide the ozone
168 partial pressure (in mPa), and temperature above each location. The sites are chosen to provide
169 observations that are typically within the PV (NY-ÅL and SOD), close to the edge of the PV
170 (LER), or always outside the PV (BOU). The BOU site is to be used as a 'control' since SSW
171 effects are not generally expected to occur at such low latitudes. The geographic location of the
172 sites, and the average percentage of time that each spends within the PV from January to April are
173 shown in graphical format in Figure 2. Data from these four sites was previously used to determine
174 the role of the PV in the reduction of ozone observed following SPEs [*Denton et al.*, 2017; 2018].

175

176 **2.2 Aura/MLS satellite data**

177 The Aura satellite was launched in 2004 and carries a Microwave Limb Sounder (MLS) instrument
178 that is designed to measure the temperature and abundance of a wide range of the upper
179 stratospheric and mesospheric constituents, including O₃. A previous MLS instrument with very
180 similar characteristics was flown on the Upper Atmosphere Research Satellite [*Waters et al.*, 1999].
181 Verification methodology for the instrument can be found in the works of *Jiang et al.* [2007] and
182 *Livesey et al.* [2008]. Here, we use the vertical profile O₃ volume-mixing-ratio data (combined
183 with geopotential height data) above site-specific ground stations (L2, V04) to determine any
184 observed trends and to quantify the morphology of ozone before, during, and after SSW events.
185 These data have already been used in numerous studies of O₃ behaviour in the stratosphere and

186 mesosphere (e.g. *Manney et al.* [2006], *Boyd et al.* [2007], *Jackson and Orsolini* [2008], *Strahan et*
187 *al.* [2013], *Damiani et al.* [2014], *Kishgore et al.* [2016]).

188

189 **2.3 SAOZ ground-based UV-visible spectrometer data**

190 The Network for the Detection of Atmospheric Composition Change (NDACC) operated (Système
191 d'Analyse par Observation Zénithale) SAOZ instrument [*Pommereau and Goutail*, 1988] is
192 situated at Sodankylä and co-located with the SOD ozonesonde launch site. The instrument is a
193 UV-visible spectrometer that provides morning and evening vertical column integrals of the
194 abundance of NO₂ and O₃ that have been used in numerous observational campaigns [*Vaughan et*
195 *al.*, 1997; *Vandaele et al.*, 2005; *Pommereau et al.*, 2013]. Here, the SAOZ data are used to
196 provide: (a) an independent comparison dataset against which to test the O₃ observations from
197 ozonesondes and Aura/MLS, and (b) to determine any change in total column NO₂ from before,
198 during, and after SSWs (cf. *Ageyeva et al.* [2017]).

199

200 **2.4 SLICE meteor radar data**

201 A SkiYMET meteor radar known as the Sodankylä-Leicester Ionospheric Coupling Experiment
202 (SLICE) was installed in northern Finland in 2008, positioned at the same location as the SOD
203 ozonesonde launching site discussed above. The instrument transmits at ~36.9 MHz and
204 subsequently measures the Doppler shift of returning echoes from meteors in the upper atmosphere.
205 The meridional and zonal wind speeds in the altitude region from ~80-100 km (upper mesosphere -
206 lower thermosphere) may then be derived from these observations [*Hocking et al.*, 2001]. In
207 previous work *Lukianova et al.* [2015] used the SLICE radar observations during three SSWs to
208 demonstrate that mesospheric cooling occurs prior to stratospheric warming, and that the cooling
209 and warming were of similar magnitudes (~50 K). Here, we utilize the SLICE data to quantify the
210 change in zonal wind direction in the mesosphere that occurs during our set of SSWs (2008-2016).

211

212 **3. Results**

213

214 **3.1 Ozonesonde results**

215 Data from the ground-based ozonesondes introduced in Section 2.1 are not launched daily at any
216 site (Table 2 and Figure 2). Thus, none of the sites has continuous daily coverage during the 37
217 SSW-events considered here. Rather than investigate individual events, we carry out a superposed
218 epoch analysis (i.e. composite analysis) of the events to reveal the statistical characteristics of
219 SSWs. The mean O₃ volumetric mixing ratio at each site is first calculated (measurements are
220 usually recorded as O₃ partial pressure) and then plotted as a function of altitude and month and
221 shown in the left column of Figure 3. There is a clear latitudinal trend to the data with the lowest
222 latitude site (BOU) showing the highest mixing ratio and the highest latitude site (NY-ÅL) having
223 the lowest mixing ratio. Strong annual variations at each site are also evident with the highest level
224 of O₃ generally found in northern hemisphere spring and the lowest level occurring in autumn. The
225 peak O₃ mixing ratio occurs at around 30 km altitude for all sites. The mixing ratio plots presented
226 here may be compared directly with the mean ozone partial pressures previously calculated at each
227 site and plotted in Figure 2 of *Denton et al.* [2018] (see also *Kivi et al.*, 2007). The main point to
228 note is that the peak partial pressure of O₃ occurs at ~20 km altitude (the peak of the stratospheric
229 ozone layer) while the peak in the volumetric mixing ratio occurs roughly 10 km higher.

230

231 Also shown in the right column of Figure 3 are superpositions of the O₃ mixing ratio at each of the
232 four sites, with respect to the 37 SSWs (these are initially uncorrected for season). Certain trends
233 can immediately be drawn from these plots. Firstly, there is a clear latitudinal variation. The most
234 poleward site (NY-ÅL) shows clear evidence for a sharp increase in the O₃ mixing ratio following
235 the onset of SSWs. The data at SOD and LER show similar trends, although with a less clear

236 demarcation from before-SSWs to after-SSWs. There is little evidence of a clear systematic
237 variation in the data from BOU during the period under study. However, since the data plotted here
238 are not seasonally-detrended the apparent observed changes cannot be simply attributed to SSWs.
239 The SSWs generally occur at the start of the year when the underlying annual trend at all sites is for
240 an increase in the O₃ mixing ratio. It is essential that this "natural" increase is removed when the
241 underlying aim is to reveal perturbations to the annual trend that are due solely to SSWs.

242

243 To correct for seasonal biases in the data, and to quantify the variation in O₃ due solely to SSWs,
244 we again calculate the difference-from-mean at each site. Figure 4 contains these difference-from-
245 mean plots with respect to the temperature (top row), the O₃ mixing ratio (middle row) and the O₃
246 partial pressure (bottom row). The difference-from-mean of each parameter is plotted with
247 increases (above mean value) shown in shades of red and decreases (below mean value) shown in
248 shades of blue. Values close to the mean value are coloured white. Note: for the temperature,
249 changes from the mean are plotted in °C. For the O₃ mixing ratio and O₃ partial pressure, the
250 changes are plotted as a percentage increase (red) or decrease (blue) from the mean value.

251

252 With reference to the temperature, the changes that occur due to SSWs can be found in the top-row
253 of panels of Figure 4. These show numerous interesting features. At NY-ÅL (first column) there is
254 a clear increase in the measured atmospheric temperature over a wide altitude range that
255 commences close to the arrival of SSWs. The maximum difference-from-mean is ~10°C (Figure 4,
256 top left plot) while the absolute change in temperature from a few days before the SSW occurrence
257 to a few days after is ~20 °C (although again there are wide variations in these values on an event-
258 by-event basis). The temperature changes at SOD and LER are similar (although the increase is
259 slightly less than that observed at NY-ÅL) At all three sites the temperature first increases at
260 higher altitudes >30 km a few days before zero epoch. Higher temperatures are subsequently

261 detected at ~20 km altitude a few days later. Temperature changes persist for up to 40 days (NY-
262 ÅL) although these changes are somewhat altitude-dependent as expected. In contrast with the
263 more poleward locations, there are no systematic changes in temperature evident at the BOU site,
264 which is outside the PV at all times.

265

266 With reference to the O₃ mixing ratio during SSWs, the plots in the middle row of Figure 4 also
267 show clear trends. At NY-ÅL, the O₃ mixing ratio shows a clear rapid increase of ~15-20%
268 commencing around zero epoch at altitudes ~20-30 km. This persists for in excess of 30 days
269 (albeit in an altitude-dependent way). The data from SOD and LER are less clear, although the
270 mixing ratio increases to ~10% above of the mean value after zero epoch. Again, there are no
271 systematic changes in mixing ratio evident at BOU.

272

273 With reference to the O₃ partial pressure, the plots in the bottom row of Figure 4 show similar
274 features as observed for the mixing ratio. The data from NY-ÅL shows an increase of up to 30%
275 occurring at the same time as the SSW in the altitude region between ~20-30 km. This feature
276 persists for ~30-40 days. A similar magnitude increase is also observed centred on ~10 km
277 altitude, with altitudes around 15-20 km showing a less substantial increase. Again, SOD and LER
278 show some evidence of similar trends (~10% increase) but with much more variation. There are no
279 systematic trends in the O₃ partial pressure in the BOU data.

280

281 **3.2 Aura/MLS ozone results**

282 Data from the Aura/MLS instrument span the period from Aug 2004-2017 and thus include 15 of
283 the 37 events. However, although the altitudinal resolution is somewhat coarse (compared with the
284 ozonesondes) these data have the advantage of much higher temporal coverage for all of the four
285 selected locations, with daily files usually available. The Aura/MLS data shown in Figure 5

286 provide independent confirmation of the ozonesonde results (shown in Figure 3 and Figure 4) in the
287 altitudinal region of overlap, and have the added benefit of coverage in altitude up into the
288 mesosphere. Here, data are plotted from 0-80 km altitude although data at altitudes below ~215
289 hPa (~10 km altitude) should be generally disregarded [Jiang *et al.*, 2007; Livesey *et al.*, 2008].

290

291 As with the ozonesonde data, we initially calculate the mean annual variation in the O₃ mixing ratio
292 above each of the four sites and plot this with the same scale as previously used. The results of this
293 are shown in Figure 5. In the altitude region of overlap there are similar trends in the mean annual
294 variations of the Aura/MLS data as were observed by ozonesonde (cf. Figure 3). Notably, the
295 highest mixing ratio is found at the lowest latitude (BOU). The overall magnitude of the averages
296 are similar at all sites, in the altitude region of overlap. The general agreement found between
297 Aura/MLS and ECC ozonesondes provides further confidence in the comparison of MLS data with
298 ozonesonde data during SSWs, despite the MLS dataset only covering years from 2004 onwards
299 (and thus only 15 SSWs).

300

301 Figure 5 contains plots of the superposed O₃ mixing ratio observed by Aura/MLS data during 15
302 SSWs that occurred after Aug 2004. The left column in this figure shows the superposed data
303 uncorrected for season while the right column shows the same data seasonally-detrended (i.e.
304 plotted as a percentage difference-from-mean). For clarity, the difference-from-mean plots are
305 limited in altitude from the stratosphere above 20 km and the mesosphere below 60 km where data
306 reliability, coverage, and altitudinal resolution, are all greatest.

307

308 As with the ozonesonde data, it is clear that the O₃ mixing ratio undergoes a sharp and substantial
309 increase with the onset of SSWs, particularly at the highest latitude sites (NY-ÅL and SOD). The
310 mean mixing ratio is increased by ~20% at all altitudes between 20-60 km and persists upwards of

311 40 days. At LER there is some evidence of an increase in the mixing ratio following the SSWs.
312 There is no evidence of an increase in the mixing ratio at BOU. The magnitudes of the changes
313 observed by Aura/MLS (at the sites where an increase is observed) are of a similar order to that
314 seen with the ozonesondes.

315

316 **3.3 NO₂ and O₃ column integrals from SAOZ results**

317 Data from the SAOZ UV-visible spectrometer provide NO₂ and O₃ column abundances at SOD,
318 with which to further confirm the ozonesonde and MLS results for O₃, and also with which to
319 examine the effect of SSWs on total NO₂. As with other parameters, we commence by calculating
320 the mean of the parameter (measured density during both the morning and evening observations) as
321 a function of month. These are plotted in Figure 7. Both NO₂ (left column) and O₃ (right column)
322 show large annual variations during morning (top row) and evening (bottom row) which make it
323 necessary to carry out a seasonally-corrected difference-from-mean analysis to reveal changes in
324 these parameters solely due to SSWs.

325

326 Figure 8 contains plots of the superposed NO₂ and O₃ morning and evening observations as a
327 function of time relative to 36 of the 37 SSWs when data are available. The left column shows the
328 data uncorrected for season and the right column shows the superpositions seasonally-corrected as a
329 difference-from-mean value. The thick black line is the mean of the superposition while the red,
330 blue and purple lines denote the upper quartile, median, and lower quartile of the averages. In these
331 plots there is an apparent slow increase in NO₂ that commences around zero epoch. A sharper
332 increase is also evident for O₃ (both morning and evening). However, the seasonally-corrected
333 plots shown in the right column indicate the true variations linked to SSWs rather than due to the
334 background seasonal variations. The superposed NO₂ profiles for morning and evenings (top two
335 rows) are flat, indicating that the total column-integrated NO₂ at SOD is unchanged by the onset of

336 a SSW (a result in agreement with the findings of *Sofieva et al.* [2012]). In contrast, the total
337 column O_3 at SOD is actually *decreasing* prior to the SSWs. Following zero epoch there is a rapid
338 increase in total-column O_3 and elevated levels of ozone persist for in excess of 40 days. Note: We
339 also examined the column integral data from the Ozone Monitoring Instrument (OMI) on the Aura
340 satellite with the NO_2 and O_3 column data from SAOZ. The Aura/OMI data do show some
341 evidence of a similar increase in column ozone around the onset of SSWs (not shown) but data
342 from OMI at the high latitude sites are sparse due to the orbit of the satellite and thus have not been
343 considered further.

344

345 **3.4 Mesospheric winds from SLICE results**

346 The break up of the PV is generally accompanied by a sudden reversal in mean zonal wind
347 direction in the stratosphere and mesosphere. In order to confirm that this reversal occurs for our
348 collection of SSWs we perform a similar analysis as for the other data sets using data from the
349 SLICE meteor radar. Hence we can quantify the change in zonal wind speed at the very top of the
350 mesosphere and close to the mesopause, at the SOD site between 82 and 100 km altitude (data
351 above 100 km altitude were unavailable during these intervals). Figure 9 shows a superposition of
352 the zonal wind speed as a function of time from the onset of SSW for 9 of the 37 SSW events after
353 2008 when data are available. This figure shows wind with a west-to-east direction as having a
354 positive zonal wind speed (red) and an east-to-west direction as having a negative zonal wind speed
355 (blue). Despite the limited SSW dataset, a robust trend is evident. Strong positive wind speeds
356 (west-to-east) occur until a few days prior to zero epoch. West-to-east winds at SOD are indicative
357 of the anti-clockwise PV winds over the northern pole during winter (cf. Figure 1 of *Denton et al.*,
358 2018]) The zonal wind direction ceases to be strongly westwards-to-eastwards a few days prior to
359 zero epoch and then changes sharply to an east-to-west direction suddenly, very close to zero
360 epoch, confirming the disruption/break-up of the PV over SOD around this time. This sharp trend

361 is (on average) short-lived, lasting only ~4 days. After zero epoch the wind direction is much more
362 variable with both easterly and westerly winds being observed, although this is somewhat
363 dependent upon altitude.

364

365 **4. Discussion**

366 Very complex (temperature-dependent) chemistry and transport governs the abundance of O₃ in the
367 stratosphere/mesosphere [e.g. *Brasseur and Solomon*, 1986; *Newman et al.*, 2001; *Tegtmeier et al.*,
368 2008a]. Elucidating how the O₃ abundance changes provides clues as to the most important of
369 these processes before, during, and after SSWs. The results of the current study, documented
370 above, provide quantification of the statistical changes typically occurring in various physical
371 parameters during SSWs, with reference to the mean state of the stratosphere and mesosphere.

372

373 For the 37 SSWs studied here the in-situ balloon ozonesonde observations at four sites demonstrate
374 an increase in the mean temperature at the highest latitude site (NY-ÅL) of ~10°C at stratospheric
375 altitudes of ~15-30 km (Figure 4, top left panel). Lower-latitude sites (SOD and LER) show a
376 similar, although less strong, increase as might be expected - these sites are not always within the
377 PV during the winter months (see Table 2). The volume mixing ratio at NY-ÅL increases by ~20%
378 above the mean at the onset of the SSWs with a slightly lower increase observed at SOD and LER.
379 No increase in temperature, O₃ mixing ratio, or O₃ partial pressure are observed at the control-site
380 of BOU, which is consistently outside the PV.

381

382 The mean upper stratospheric/mesospheric O₃ mixing ratios, as measured by Aura/MLS, are shown
383 in Figure 5. The absolute change and the difference-from-mean changes in these satellite-measured
384 parameters during SSWs are shown in Figure 6. The increase in O₃ mixing ratio at NY-ÅL and
385 SOD (~20% in the altitude region 20-60 km) following the SSWs agrees very well with the

386 ozonesonde observations, in the overlapping altitude region. As noted above, the larger altitude
387 range provided by the satellite observations also provides additional insights into the altitude range
388 of the SSW-linked changes.

389

390 The average annual variation of total-column NO_2 and O_3 at Sodankylä are shown in Figure 7. The
391 difference-from-mean of these constituents (Figure 8) clearly shows that the total-column NO_2 is
392 completely unchanged by SSWs while total-column O_3 undergoes a sharp increase. Of course, our
393 results do not provide any information regarding the *altitudinal distribution* of NO_2 during SSWs.
394 It is perfectly possible (and perhaps likely) that the altitudinal distribution of NO_2 will change
395 during SSWs. However, investigation into changes in the composition during SSWs were
396 previously carried out for the stratosphere, mesosphere, and lower thermosphere by *Sofiieva et al.*
397 [2012]. The authors used GOMOS data to show that enhancements in NO_3 were strongly
398 (positively) correlated with the temperature changes that followed SSWs (during 2003-2008),
399 although there were no clear changes noted in NO_2 [*Sofiieva et al.*, 2012] - in agreement with
400 findings in the current study.

401

402 The decrease in total-column O_3 before SSWs, also shown in Figure 8, is indicative of the usual
403 polar-night chemical loss (dominated by NO_x and O_3 chemistry) due to the presence of a PV. Once
404 such losses cease, at the onset of the SSW, then O_3 increases rapidly (since the main loss
405 mechanism is absent while the transport of ozone continues - cf. Figure 1). Finally, the meteor
406 radar observations at SOD confirm the clear reversal in mesospheric zonal wind direction that
407 occurs at the onset of the SSWs used in this study (Figure 10 - cf. *Lukianova et al.*, 2015).

408

409 In the context of previously published work, the results presented in this study have provided
410 observational statistical quantification of the increases of upper stratospheric and mesospheric

411 ozone following SSWs. For the major SSW in 2009, *Tao et al.* [2015] conclude that after the
412 event, poleward transport increased with this particular SSW accelerating the polar descent and
413 tropical ascent of the Brewer–Dobson circulation, and thus leading to the rapid increase in
414 stratospheric O₃. The importance of this "resupply" of ozone into the polar stratosphere was also
415 highlighted by *Manney et al.* [2011] following the exceptional loss of Arctic ozone in 2011.

416

417 The work of *de la Cámara et al.* [2018a] provides particularly robust analysis of the changes
418 expected during SSWs based on results from the Whole Atmosphere Community Climate Model
419 (WACCM) version 4. In that study the authors discuss the change in O₃ in terms of the continuity
420 equation of ozone concentration in WACCM and attribute the observed O₃ increase as being due to
421 the temporal offset between ozone eddy transport and diffusive ozone fluxes. Despite the different
422 scales, there are clear similarities between the average O₃ changes occurring following SSWs
423 presented in Figure 6 of this current study and the O₃ changes plotted in Figure 3 in *de la Cámara*
424 *et al.* [2018a], which add further observational evidence for their conclusions.

425

426 Our previous work on stratospheric ozone considered the effects of SPEs on stratospheric ozone
427 during the polar winter, and the role of the PV upon the chemical destruction of O₃ [*Denton et al.*,
428 2017; 2018]. These statistical studies showed clear statistical losses in stratospheric O₃ following
429 SPEs but the analysis gave no consideration to years with, or without, a SSW. The differing roles
430 of SPEs and SSWs have also been investigated by *Päivärinta et al.* [2013]. They showed that
431 following a SSW, a strong PV reformed and that this PV could lead to enhanced downwards
432 transport of NO_x species. There is also evidence that descent rates at the vortex edge may be much
433 greater than descent rates in the main PV [*Tegtmeier et al.*, 2008b]. SPEs generally create NO_x
434 species at mesospheric (and/or upper stratospheric) altitudes [*Seppälä et al.*, 2008]. These species
435 then descend in the PV and cause chemical destruction of O₃ in the stratosphere/lower-mesosphere.

436 In contrast, and as shown here, SSWs cause a disruption of the PV and subsequent increases in O₃.
437 These two competing effects need to be independently determined and here modelling work is
438 essential. A complicating issue for event studies is the state of the atmosphere prior to an event
439 such as an SSW or SPE. The study of *de la Cámara et al.* [2017] indicated that conditions in the
440 stratosphere prior to a SSW event were important in the evolution/occurrence of the SSW.

441

442 In contrast to examining the geographic distribution of O₃, we are unaware of any definitive study
443 where the vorticity of the atmosphere is treated explicitly in the data analysis. For such a study, the
444 analysis could proceed with the data ordered with respect to *vorticity* rather than *geographic*
445 *position*. For example, H₂O is a good tracer for the PV in the stratosphere/mesosphere, having a
446 low mixing ratio inside the vortex [*Scheiben et al.*, 2012]. Our current and future work is focused
447 on exploring such explicit connections between O₃ and the polar vortex location. While direct
448 concurrent observations of vorticity and O₃ may be sparse, reanalysis datasets (e.g. MERRA2,
449 ERA-Interim/ERA-5, JRA55) can provide a statistical means to better reveal connections between
450 O₃ and the polar vortex.. However, as noted by *Butler et al.* [2015], such reanalysis data sets rely
451 on satellite observations of back-scattered sunlight and during darkness these data sets rely heavily
452 on the underlying model, and thus must be used with full knowledge of their assumptions and
453 limitations. Our future work is also intended to reveal any differences that may occur in the
454 downwards transport of NO_x (and other) species from the main PV and from the edge of the PV.

455

456 Understanding (and accurately modelling) changes in the atmosphere during SSWs remains an
457 important and timely issue [e.g. *Tripathi et al.*, 2015, *Kretschmer, et al.*, 2018, *Pedatella et al.*,
458 2018]. The frequency and strength of SSWs have also been discussed as factors in how
459 anthropogenic and/or long-term climatic changes in the atmosphere are manifested (e.g.
460 *Kuttippurath and Nikulin* [2012]). This current study has quantified the changes that occur in the

461 atmosphere during SSWs, with respect to the underlying annual changes. This is particularly
462 necessary in order to allow direct model-to-data comparison, once seasonal detrending of the data
463 have been carried out.

464

465 **5. Conclusions and Summary**

466 To conclude, the work carried out in this study has quantified the changes occurring in the O₃
467 mixing ratio, temperature, total-column O₃, total-column NO₂, and mesospheric winds during 37
468 SSWs between 1989 and 2016 (or subsets thereof due to the availability of experimental data)
469 Using the superposed-epoch technique has allowed the changes that occur due to SSWs to be
470 identified with respect to the natural underlying variability.

471

472 The main findings of this study, in relation to the 37 SSWs in this study, are summarized below:

473

474 **1. Locations consistently inside the PV show strong changes linked to the timing of SSWs.**
475 **Changes are less evident for sites occasionally inside the PV, and no changes are observed at**
476 **sites consistently outside the PV.**

477

478 **2. A sudden increase in mean temperature (prior to the SSW) is first observed at ~60 km**
479 **altitude and subsequently at lower altitudes for the two high-latitude sites. The average**
480 **duration of the temperature increase at these sites is ~40 days.**

481

482 **3. An increase in O₃ (of ~20% above the monthly mean) is observed at the two highest**
483 **latitude sites. This persists for ~40 days. There is good agreement between the statistical**
484 **ozonesonde observations and the Aura/MLS observations.**

485

486 **4. The total-column NO₂ is unchanged during SSWs. The total-column O₃ decreases prior to**
487 **zero-epoch and then increases sharply. This increase persists for in excess of 40 days.**

488

489 **6. Acknowledgements**

490 Ozonesonde data used in this study were retrieved from the World Ozone and Ultraviolet Radiation
491 Data Centre (<https://woudc.org/>). We thank David Moore, Peter von der Gathen, and Bryan
492 Johnson for provision of the data used here. Aura/MLS data may be retrieved from the NASA Data
493 and Information Services Center (<https://daac.gsfc.nasa.gov/>) and we thank all members of the
494 MLS team for provision of the data. SAOZ spectrometer data used here are available online
495 (<http://saoz.obs.uvsq.fr>) and we thank J-P. Pommereau and F. Goutail for their provision. SLICE
496 meteor-radar data are available by contacting Thomas Ulich at SGO (thomas.ulich@sgo.fi).

497

498 MHD is supported by NSF GEM program award number 1502947 and NASA Living With A Star
499 grants NNX16AB83G, NNX16AB75G and 80NSSC17K0682. Research at FMI was supported by
500 the Academy of Finland (grant number 140408); an EU Project GAIA-CLIM; the ESA's Climate
501 Change Initiative programme and the Ozone_cci sub-project in particular. We thank NASA and
502 NSSDC for the Earth images used in Figures 1 and 2,. MHD wishes to thank Niel Malan for wise
503 words and especially thank all at the FMI Arctic Research Centre, the Sodankylä Geophysical
504 Observatory, and the SSC for their hospitality during his visit to Sodankylä in the spring of 2018.

505

506

YEAR	MONTH	DAY	DAY OF YEAR
1989	2	21	52
1990	2	12	43
1991	2	4	35
1992	1	13	13
1993	3	7	66
1994	1	3	3
1994	3	29	88
1995	2	3	34
1995	3	22	81
1996	3	29	89
1997	12	24	358
1998	3	28	87
1998	12	14	348
1999	2	24	55
2000	3	19	79
2000	12	20	355
2001	1	2	2
2001	2	10	41
2001	12	27	361
2002	2	16	47
2003	1	17	17
2004	1	3	3
2005	2	1	32
2005	3	11	70
2006	1	20	20
2007	1	2	2
2007	2	22	53
2008	2	21	52
2009	1	23	23
2010	1	26	26
2011	2	1	32
2011	3	25	84
2012	1	17	17
2013	1	17	17
2014	3	31	91
2015	1	5	5
2016	3	16	76

507

508 **TABLE 1:** *Dates of SSWs used in the analysis and taken from Table 2 of Butler et al. [2017] and*509 *Table 4.1 in Ehrmann [2012].*

510

511

Site	Latitude (GLAT)	Longitude (GLON)	# Ozonesondes in Analysis (Range)	Polar Vortex (PV) in Winter ?	Reference
Ny-Ålesund	78.90	12.00	2350 (1991-2016)	Usually within PV (>70% of time)	<i>Rex et al. [2000]</i>
Sodankylä	67.37	26.63	1886 (1989-2016)	Usually within PV (>50% of time)	<i>Kivi et al. [2007]</i>
Lerwick	60.15	-1.15	1289 (1994-2016)	Occasionally within PV (~15% of time)	<i>Smedley et al. [2012]</i>
Boulder	40.01	-105.27	1287 (1991-2016)	Never Within PV (0% of time)	<i>Johnson et al. [2002]</i>

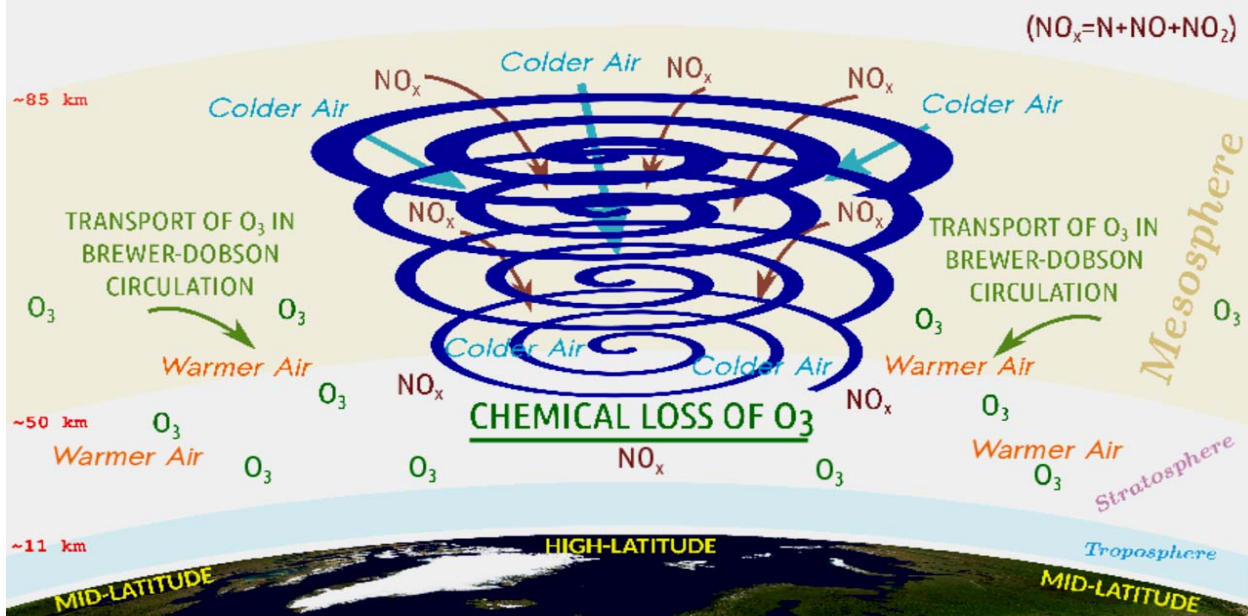
512

513 **TABLE 2:** Location of sites used in this analysis with the corresponding range of data available at
514 each site.

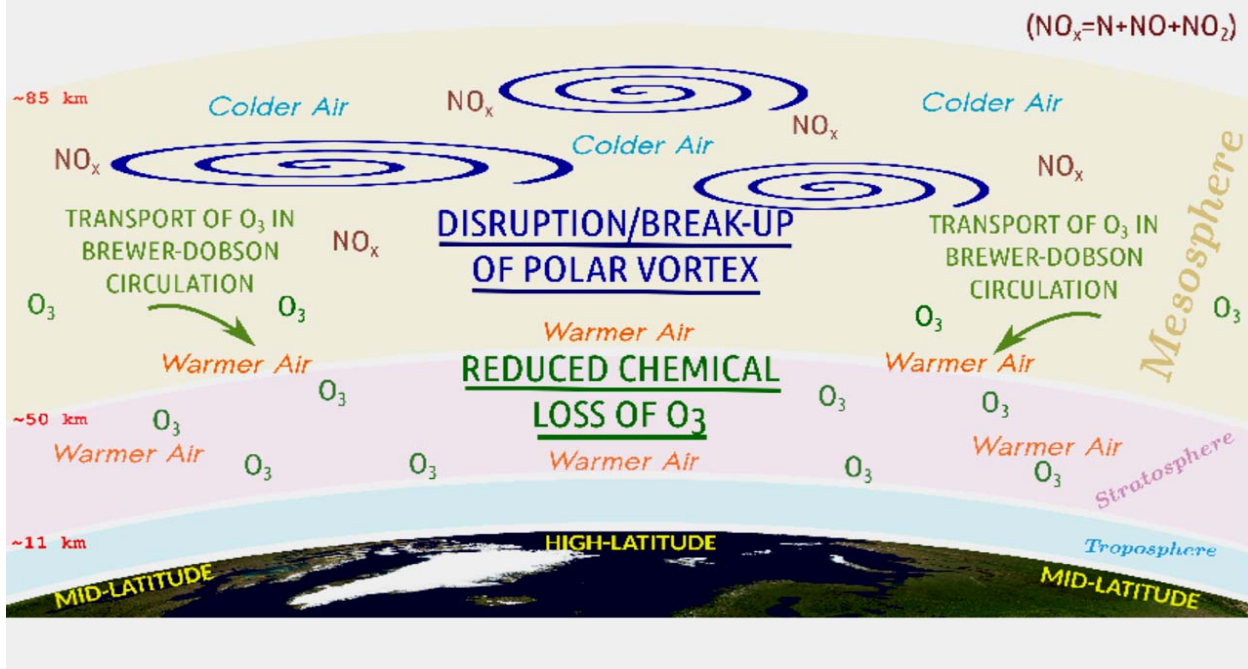
515

516

TYPICAL WINTER TRANSPORT IN THE NORTHERN HEMISPHERE



THE NORTHERN HEMISPHERE FOLLOWING A SUDDEN STRATOSPHERIC WARMING



517

518

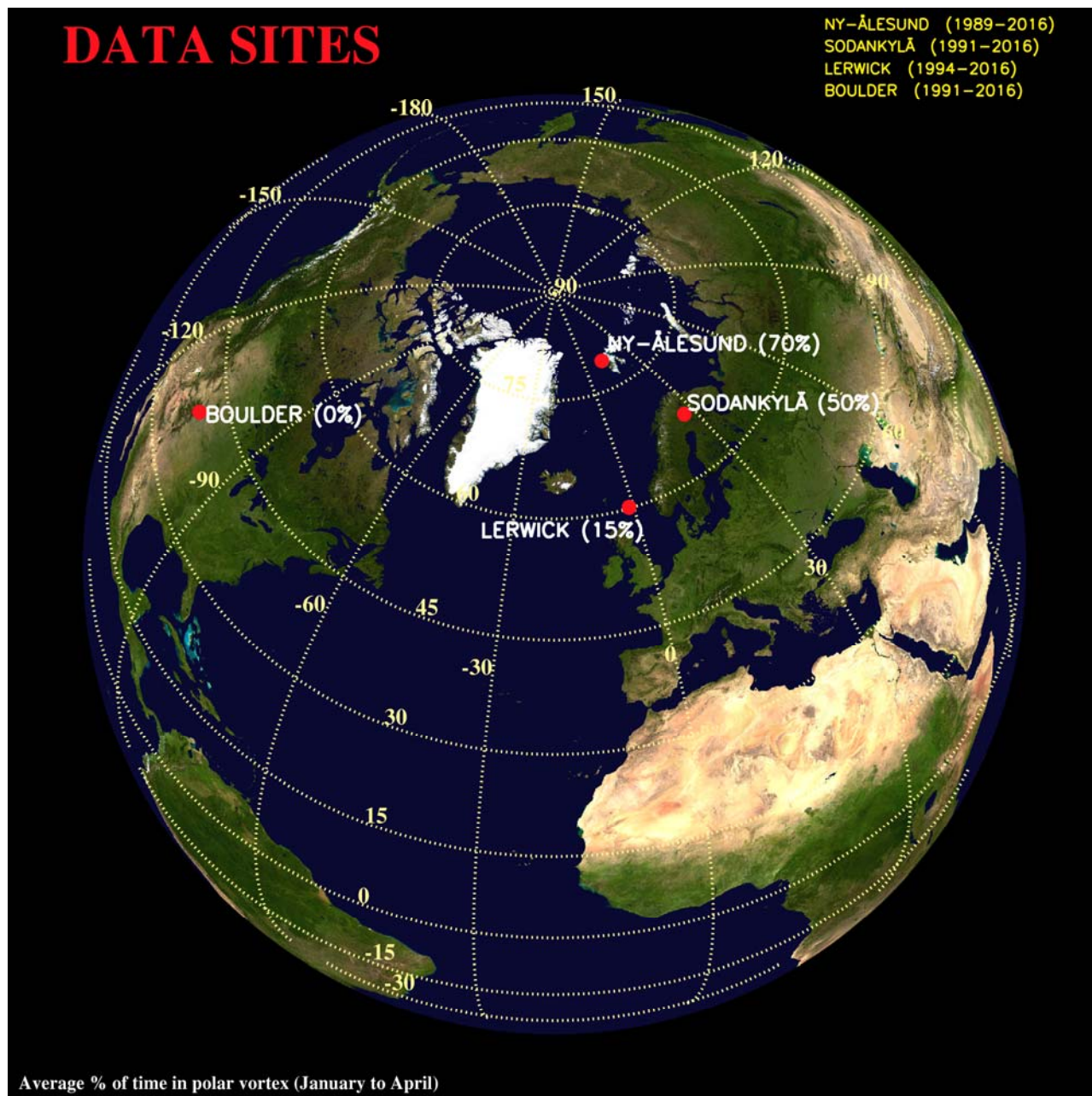
519

520

521

Figure 1. Atmospheric processes in the northern hemisphere (top) and some of the changes that occur during SSWs (bottom). The strength of the polar vortex (dark-blue/purple) is closely linked to the amount of ozone in the stratosphere/mesosphere (Figure created via Inkscape).

522

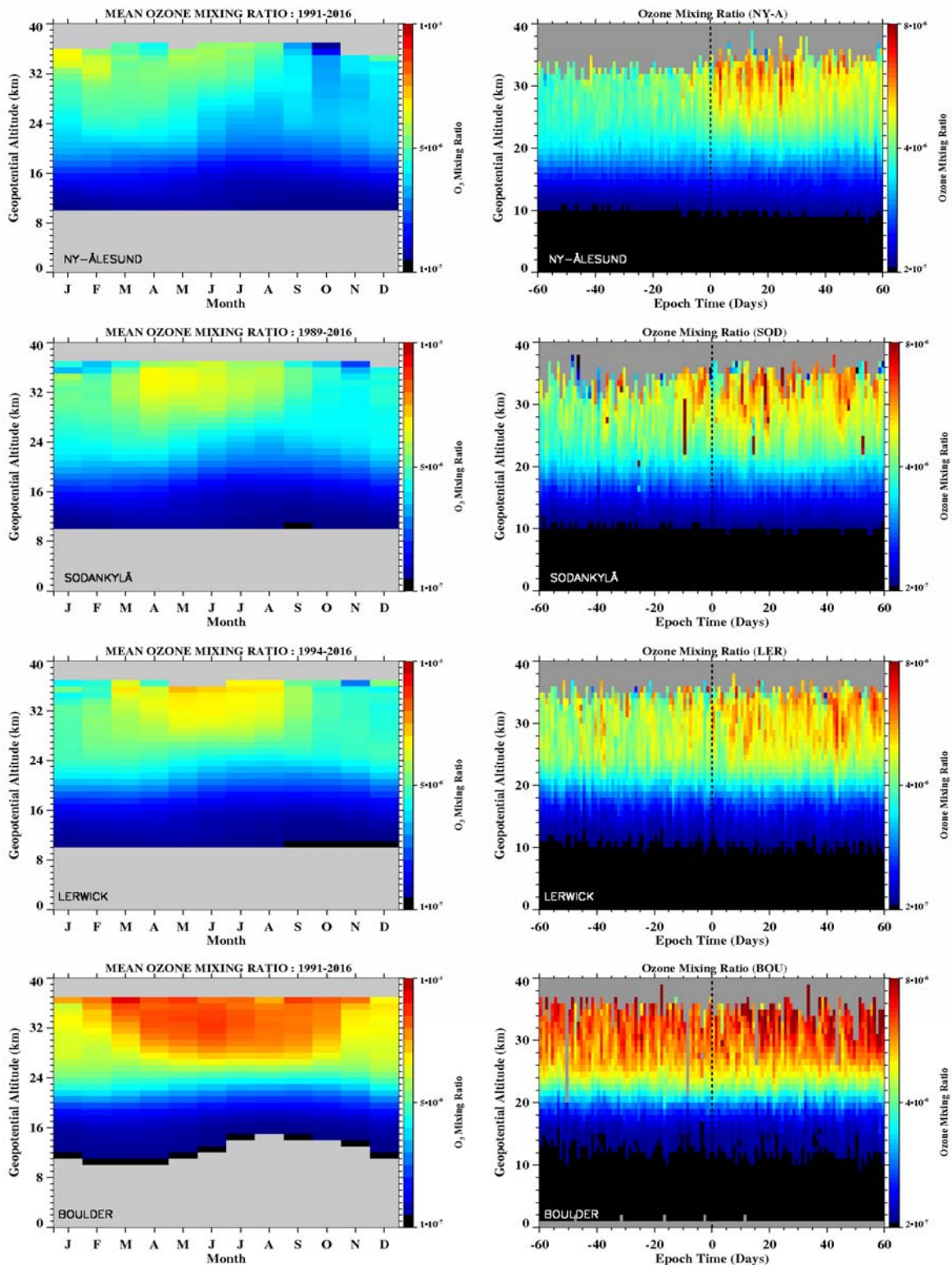


523

524

525 **Figure 2.** Location of ground stations in the northern hemisphere used in the analyses (Figure
 526 created with IDL).

527



529

530

Figure 3. Showing the mean ozone mixing ratio as a function of altitude (left column) for four sites

in the northern hemisphere. Also showing the superposed change in mixing ratio at each site (right

column) for the 37 SSWs. Data at the three northern-most sites (NY-ÅL, SOD, LER)) show an

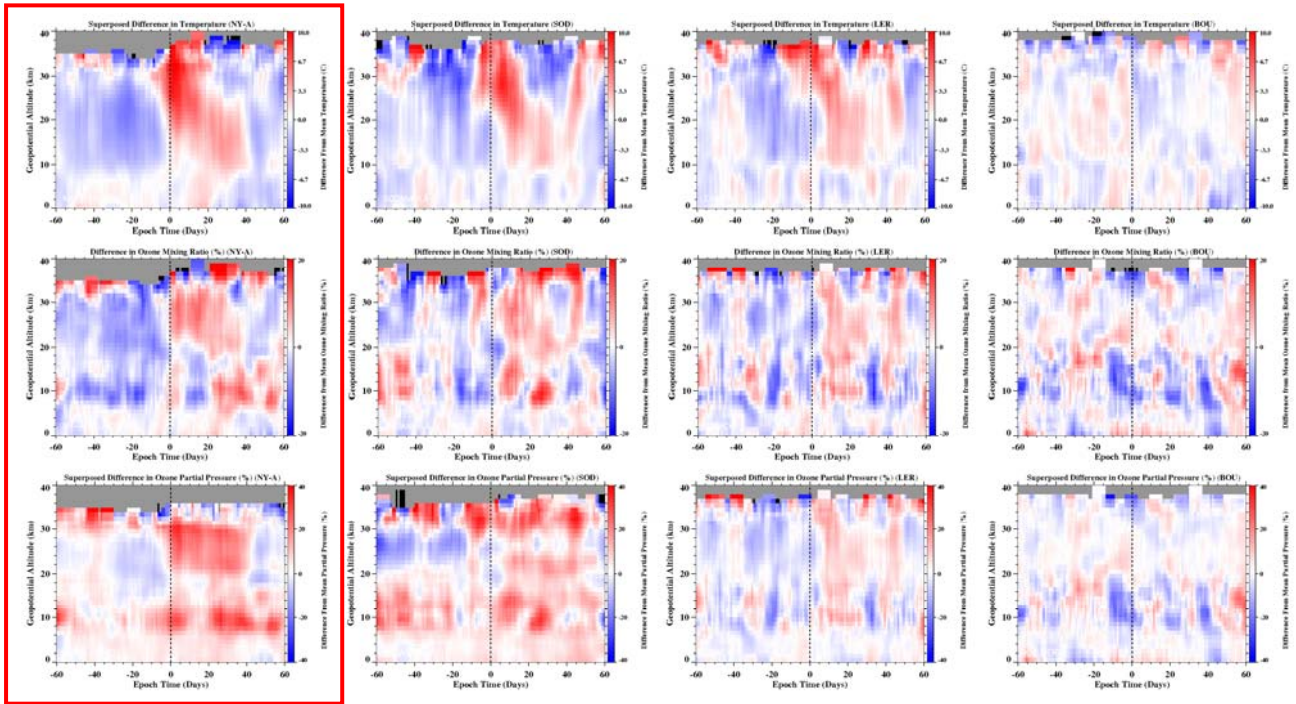
increase in ozone commencing with the start of the SSW events. Data from the most southerly site

(BOU) show little evidence of a clear trend.

535

536

537



538

539

540

541

542

543

544

545

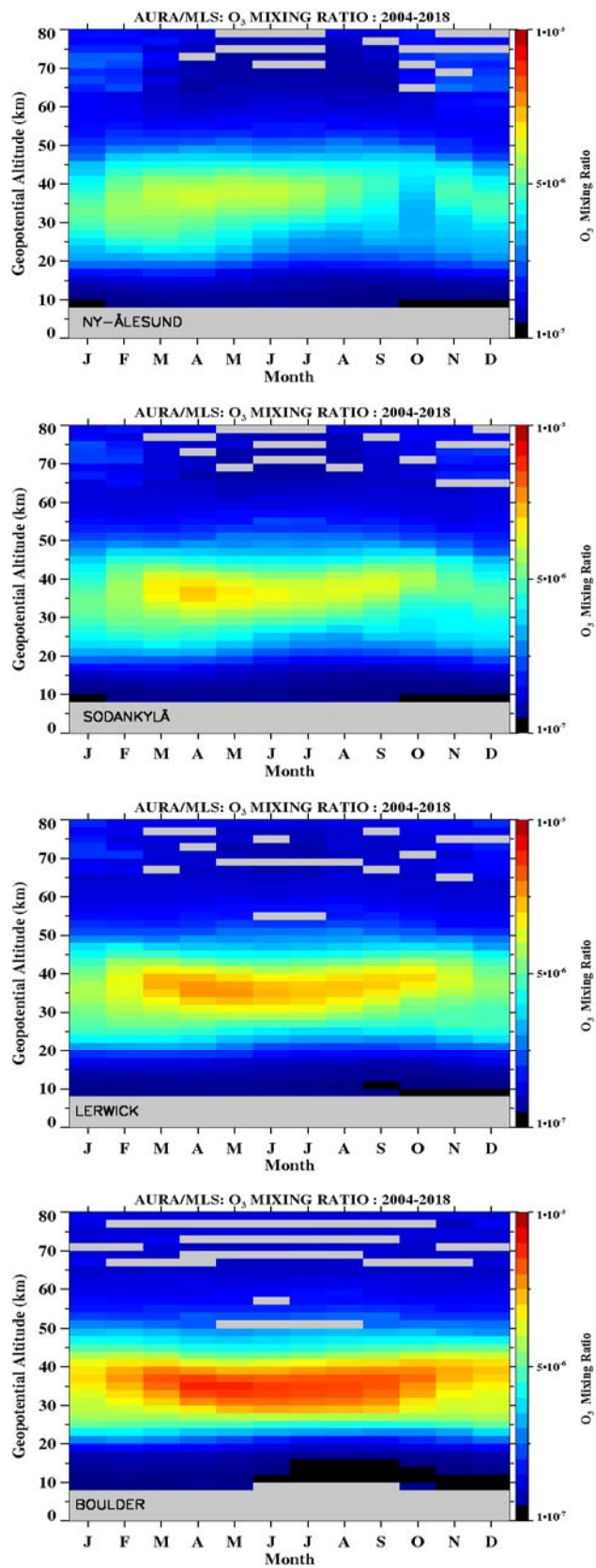
546

547

548

549

Figure 4. Showing the superposed difference-from-mean (i.e. seasonally adjusted) ozonesonde data, superposed for the 37 SSWs. Superpositions of changes in the temperature (top row), O_3 mixing ratio (middle row) and O_3 partial pressure (bottom row) are plotted at each site. Data at the three northern-most sites (NY-ÅL, SOD, LER) show some evidence for an increase in O_3 at the onset of the SSWs with a corresponding increase in O_3 mixing ratio and partial pressure also evident. The clearest changes are observed at NY-ÅL (red box) Data from the most southerly site (BOU) show no evidence of a clear trend in temperature or O_3 .



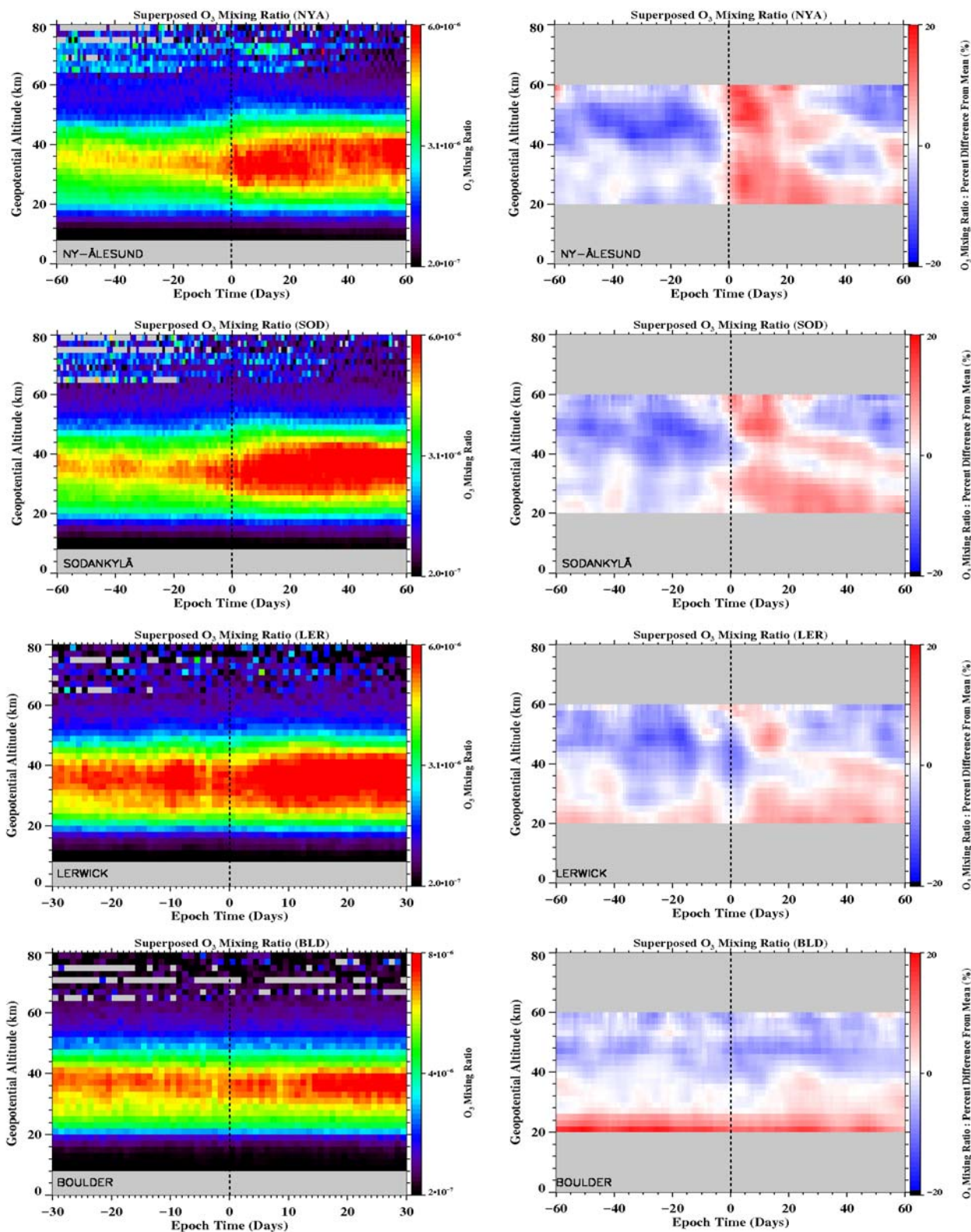
551

552

553 **Figure 5.** Showing the mean O₃ mixing ratio measured by Aura/MLS for the four sites as a

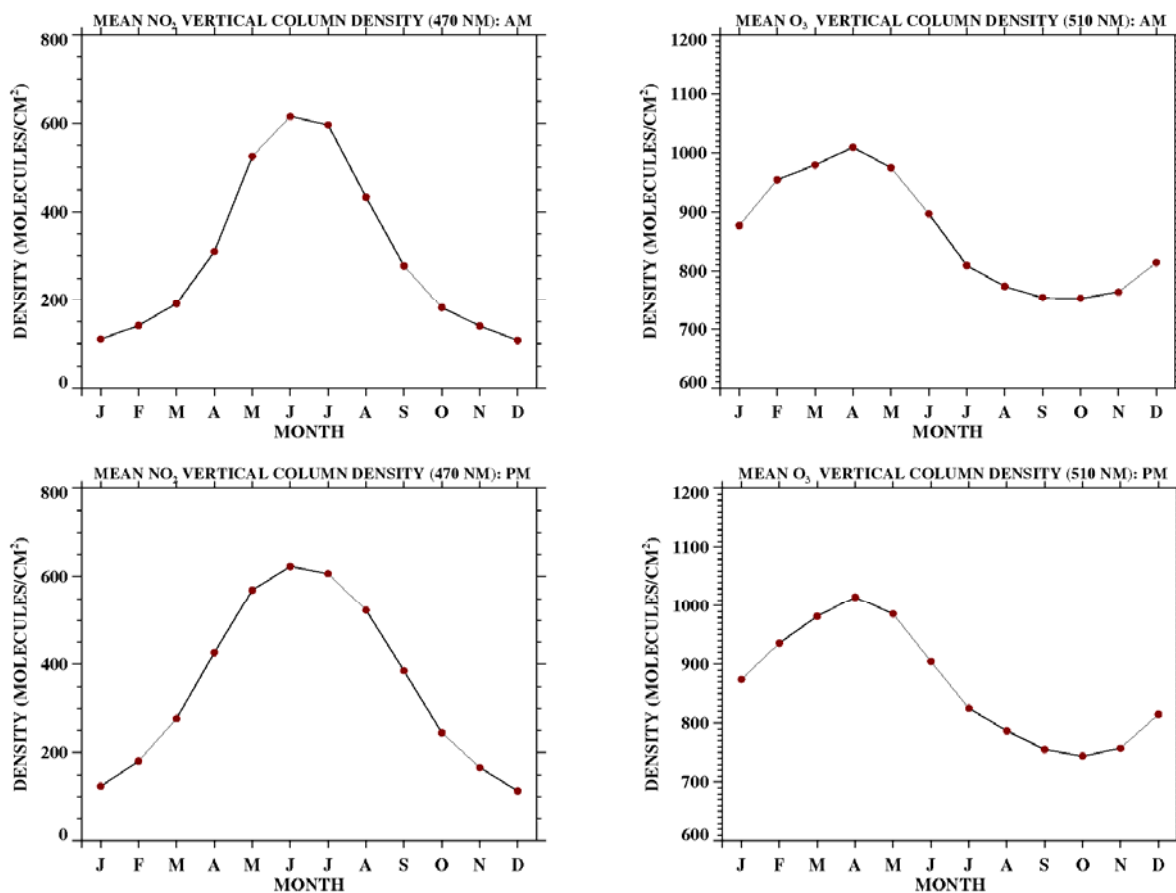
554 function of altitude and month.

555

556
557

558 **Figure 6.** Showing the superposed O₃ mixing ratio measured by Aura/MLS at the four sites for 15
 559 SSW events. The left column is the data without any seasonal correction and the right column is
 560 the change from the mean value (seasonally-corrected). The clearest changes are evident for the
 561 highest latitude sites where the O₃ mixing ratio increases substantially at the onset of SSWs.

562

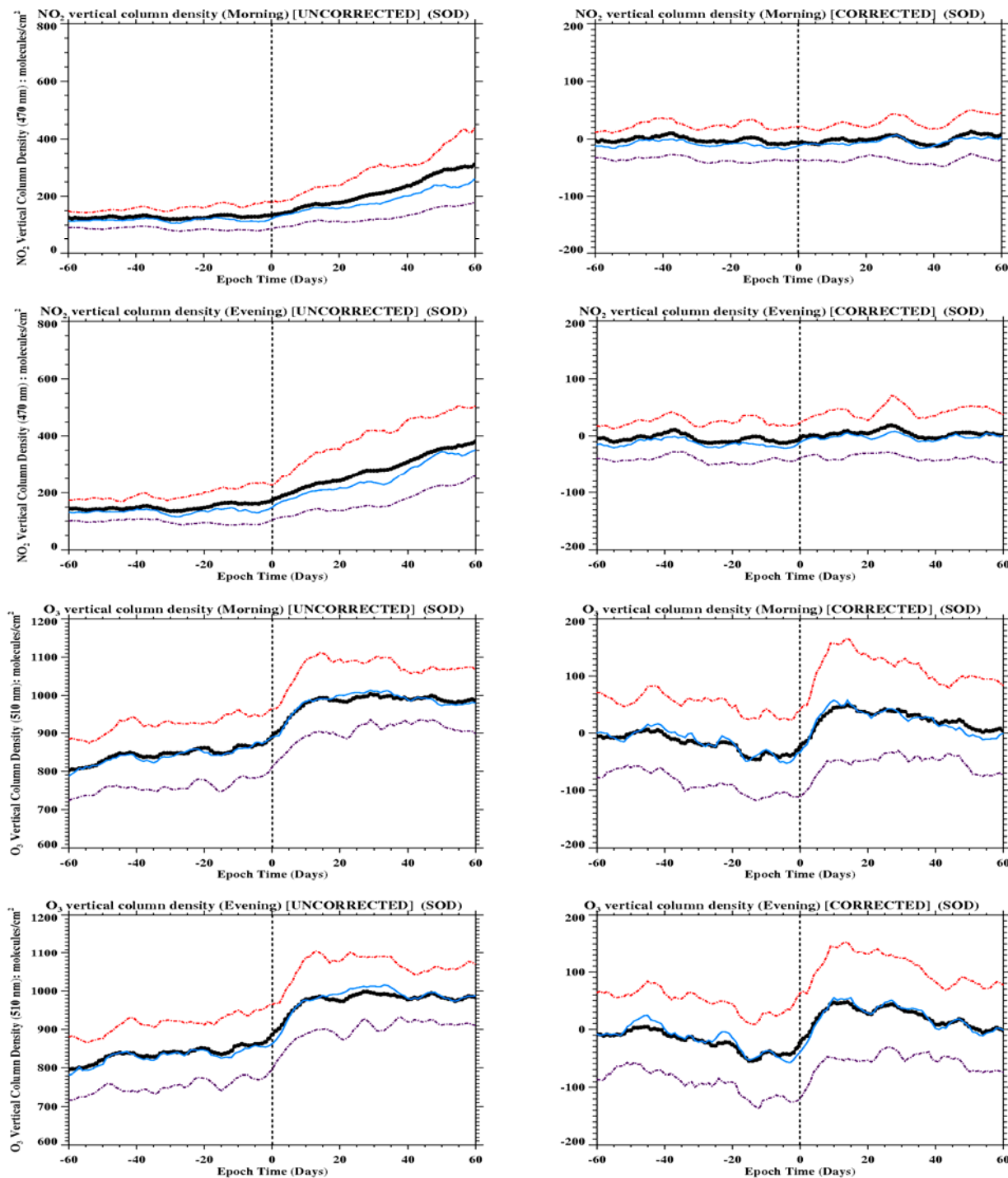


563

564

565 **Figure 7.** Showing vertical column density of NO₂ (left) and O₃ (right) above Sodankylä as
 566 measured by the SAOZ UV-visible spectrometer during morning (top) and evening (bottom)
 567 observations. There are large annual variations in each parameter.
 568

569



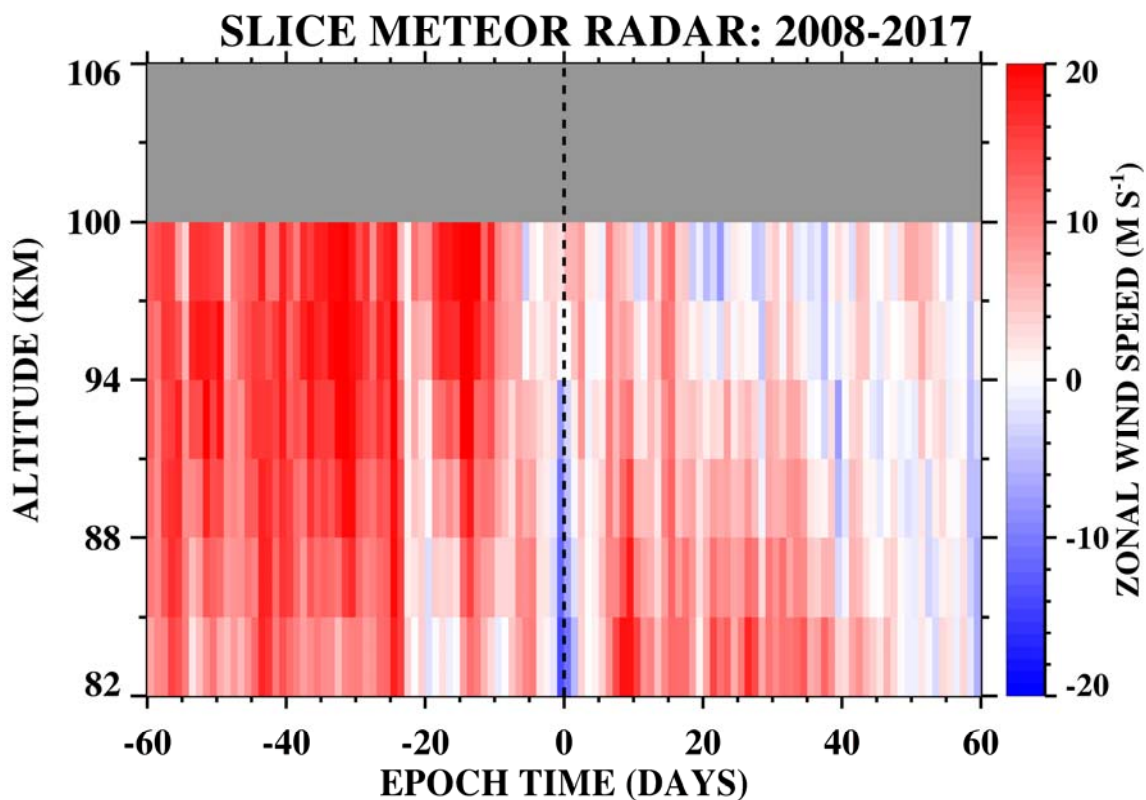
570

571

572 **Figure 8.** Showing the superposed vertical column density of NO_2 and O_3 above Sodankylä during
 573 36 SSWs occurring after 1989. The thick black line is the mean of the superposition while the red,
 574 blue and purple lines denote the upper quartile, median, and lower quartile of the averages. The
 575 left column shows each superposed parameter with no seasonal correction. The right column
 576 shows each superposed parameter as a difference-from-mean value. The seasonal corrections
 577 applied here demonstrate that NO_2 is little changed by the arrival of SSWs. In contrast O_3 appears
 578 to decrease slightly prior to the SSWs and then increases substantially following the SSW onset.

579

580



581

582

583 **Figure 9.** Showing the zonal wind speed (west-to-east) measured above Sodankylä by the SLICE
 584 meteor radar as a function of epoch time and altitude for 9 SSWs that occur after 2008. There is a
 585 sharp reversal in wind direction at the onset of the SSWs.

586

587

588

589 **References**

- 590
591 de la Cámara, A., J. R. Albers, T. Birner, R. R. Garcia, P. Hitchcock, D. E. Kinnison, and A. K.
592 Smith, *J. Atmos. Sci.*, 74, 2857-2877, 2017.
593
594 de la Cámara, A., M. Abalos, P. Hitchcock, N. Calvo, and R. R. Garcia, Response of Arctic ozone
595 to sudden stratospheric warmings, *Atmos. Chem. Phys.*, 18, 16499-16513, 2018a.
596
597 de la Cámara, A., M. Abalos, and P. Hitchcock, Changes in stratospheric transport and mixing
598 during sudden stratospheric warmings, *J. Geophys. Res. Atmos.*, 123, 3356-3373, 2018b.
599
600 Ageyeva, V.Y., A. N. Gruzdev, A. S., Elokhov, I.I. Mokhov, and N.E. Zueva, Sudden stratospheric
601 warmings: statistical characteristics and influence on NO₂ and O₃ total contents, *Izv. Atmos.*
602 *Ocean. Phys.* (2017) 53: 477, 2017.
603
604 Blum, L., X. Li, and M. H. Denton, Rapid MeV electron precipitation as observed by
605 SAMPEX/HILT during high speed stream driven storms, *J. Geophys. Res.*, 120, 3783–3794,
606 doi:10.1002/2014JA020633, 2015.
607
608 Boyd, I., A. Parrish, L. Froidevaux, T. von Clarmann, E. Kyrölä, J. Russell, and J. Zawodny,
609 Ground-based microwave ozone radiometer measurements compared with Aura-MLS v2.2 and
610 other instruments at two Network for Detection of Atmospheric Composition Change sites, *J.*
611 *Geophys. Res.* 112, D24, doi:10.1029/2007jd008720, 2007
612
613 Brasseur, G., and S. Solomon, *Aeronomy of the Middle Atmosphere*, 2nd ed., D. Reidel, Norwell,
614 Mass., 1986.
615
616 Brewer, A. W. Evidence for a world circulation provided by the measurements of helium and water
617 vapour distribution in the stratosphere, *Q. J. R. Meteorol. Soc.*, 75, 351-363, 1949.
618
619 Butchart, N., The Brewer-Dobson circulation, *Rev. Geophys.*, 52, doi:10.1002/2013RG000448,
620 2014.
621
622 Butler, A. H., D. J. Seidel, S. C. Hardiman, N. Butchart, T. Birner, and A. Match, Defining sudden
623 stratospheric warmings, *B. Am. Meteorol. Soc.*, 96, No. 11, 1913-1928, 2015.
624
625 Butler, A. H., J. P. Sjoberg, D. J. Seidel, and K. H. Rosenlof, A sudden stratospheric warming
626 compendium, *Earth Syst. Sci. Data*, 9, 63-76, 2017.
627
628 Chau, J. L., L. P. Goncharenko, B. G. Fejer, and H-L Liu, Equatorial and Low Latitude Ionospheric
629 Effects During Sudden Stratospheric Warming Events, *Space Sci. Rev.*, 168, 385-417, 2012.
630
631 Damiani, A., B. Funke, M. López Puertas, A. Gardini, T. von Clarmann, M. L. Santee, L.
632 Froidevaux, and R. R. Cordero, Changes in the composition of the northern polar upper
633 stratosphere in February 2009 after a sudden stratospheric warming, *J. Geophys. Res. Atmos.*,
634 119, 11,429–11,444, 2014.
635
636 Denton, M. H., R. Kivi, T. Ulich, M. A. Clilverd, C. J. Rodger, and P. von der Gathen Northern
637 hemisphere stratospheric ozone depletion caused by solar proton events: The role of the polar
638 vortex, *Geophys. Res. Lett.*, 45, doi:10.1002/2017GL075966, 2018.

- 639
640 Denton, M. H., R. Kivi, T. Ulich, C. J. Rodger, M. A. Clilverd, R. B. Horne, and A. J. Kavanagh,
641 Solar proton events and stratospheric ozone depletion over northern Finland, *J. Atmos. Sol-
642 Terr. Phys.*, 10.1016/j.jastp.2017.07.00, 2017.
643
- 644 Denton, M. H., and J. E. Borovsky, Magnetosphere response to high-speed solar-wind streams: A
645 comparison of weak and strong driving and the importance of extended periods of fast solar
646 wind, *J. Geophys. Res.*, 117, A00L05, doi:10.1029/2011JA017124, 2012.
647
- 648 Deshler, T., Stübi, R., Schmidlin, F. J., Mercer, J. L., Smit, H. G. J., Johnson, B. J., Kivi, R., and
649 Nardi, B.: Methods to homogenize electrochemical concentration cell (ECC) ozonesonde
650 measurements across changes in sensing solution concentration or ozonesonde manufacturer,
651 *Atmos. Meas. Tech.*, 10, 2021-2043, <https://doi.org/10.5194/amt-10-2021-2017>, 2017
652
- 653 Deshler, T., J. L. Mercer, H. G. J. Smit, R. Stubi, G. Levrat, B. J. Johnson, S. J. Oltmans, R. Kivi,
654 A. M. Thomson, J. Witte, J. Davies, F. J. Schmidlin, G. Brothers, and T. Sasaki, Atmospheric
655 comparison of electrochemical cell ozonesondes from different manufacturers, and with
656 different cathode solution strengths: The Balloon Experiment on Standards for Ozonesondes, *J.
657 Geophys. Res.*, 113, D04307, doi:10.1029/2007JD008975, 2008.
658
- 659 Dobson, G., Origin and distribution of the polyatomic molecules in the atmosphere. Proceedings of
660 the Royal Society of London. Series A, Mathematical and Physical Sciences, 236(1205), 187–
661 193, 1956.
662
- 663 Dobson, G. M., Harrison, D., & Lawrence, J., Measurements of the amount of ozone in the Earth's
664 atmosphere and its relation to other geophysical conditions. Part III. Proceedings of the Royal
665 Society of London. Series A, Containing Papers of a Mathematical and Physical Character,
666 122(790), 456–486, 1929.
667
- 668 Dütsch, H. U., and W. Braun, Daily ozone soundings during the winter months including a sudden
669 stratospheric warming, *Geophys. Res. Lett.*, 7, 10, 785-788, 1980.
670
- 671 Ehrmann, T. S., Identification and Classification of Stratospheric Sudden Warming Events,
672 Embry-Riddle Aeronautical University, Dissertations and Theses. 62, 2012.
673
- 674 Hocking, W.K., Fuller, B., Vandeppeer, B., Real-time determination of meteor-related parameters
675 utilizing modern digital technology. *J. Atmos. Sol. Terr. Phys.* 63, 155–169, 2001.
676
- 677 Jackson, D.R., and Y.J. Orsolini, Estimation of Arctic ozone loss in winter 2004/05 based on
678 assimilation of EOS MLS observations, *Q. J. Roy. Meteorol. Soc.* 134, 1833-1841,
679 doi:10.1002/qj.316, 2008.
680
- 681 Jiang, Y. B., L. Froidevaux, A. Lambert, N. J. Livesey, W. G. Read, J. W. Waters, B. Bojkov, T.
682 Leblanc, I. S. McDermid, S. Godin-Beekmann, M. J. Filipiak, R. S. Harwood, R. A. Fuller, W.
683 H. Daffer, B. J. Drouin, R. E. Cofield, D. T. Cuddy, R. F. Jarnot, B. W. Knosp, V. S. Perun, M.
684 J. Schwartz, W. V. Snyder, P. C. Stek, R. P. Thurstans, P. A. Wagner, M. Allaart, S. B.
685 Andersen, G. Bodeker, B. Calpini, H. Claude, G. Coetzee, J. Davies, H. De Backer, H. Dier,
686 M. Fujiwara, B. Johnson, H. Kelder, N. P. Leme, G. Koenig-Langlo, E. Kyro, G. Laneve, L. S.
687 Fook, J. Merrill, G. Morris, M. Newchurch, S. Oltmans, M. C. Parrondos, F. Posny, F.
688 Schmidlin, P. Skrivankova, R. Stubi, D. Tarasick, A. Thompson, V. Thouret, P. Viatte, H.

- 689 Vomel, P. von Der Gathen, M. Yela, and G. Zablocki. Validation of the Aura Microwave Limb
690 Sounder ozone by ozonesonde and lidar measurements. *J. Geophys. Res.*, 112:D24S34, 2007.
691 doi: 10.1029/2007JD008776.
692
- 693 Johnson, B. J., H. Vomel, S. J. Oltmans, H. G. J. Smit, T. Deshler and C. Kroger, Electrochemical
694 concentration cell (ECC) ozonesonde pump efficiency measurements and tests on the
695 sensitivity to ozone of buffered and unbuffered ECC sensor cathode solutions, *J. Geophys.*
696 *REs.*, 107, D19, 4393, doi:10.1029/2001JD000557, 2002.
697
- 698 Kavanagh, A. J., F. Honary, E. F. Donovan, T. Ulich, and M. H. Denton, Key features of >30 keV
699 electron precipitation during high speed solar wind streams: A superposed epoch analysis, *J.*
700 *Geophys., Res.*, 117, A00L09, doi:10.1029/2011JA017320, 2012.
701
- 702 Kivi, R., E. Kyrö, T. Turunen, N. R. P. Harris, P. von der Gathen, M. Rex, S. B. Anderson, and I.
703 Wohltmann, Ozonesonde observations in the Arctic during 1989-2003: Ozone variability and
704 trends in the lower stratosphere and free troposphere, *J. Geophys. Res.*, 112, D08306,
705 doi:10.1029/2006JD007271, 2007.
706
- 707 Kishore, P., I. Velicogna, M. V. Ratnam, G. Basha, T. B. M. J. Ourda, S. P. Namboothiri, J. H.
708 Jiang, T. C. Sutterley, G. N. Madhavi, and S. V. B. Rao, Sudden stratospheric warmings
709 observed in the last decade by satellite measurements, *Remote Sensing of Environment* 184,
710 263-275, 2016.
711
- 712 Kretschmer, M., D. Coumou, L. Agel, M. Barlow, E. Tziperman, and J. Cohen, More-persistent
713 weak stratospheric polar vortex states linked to cold extremes, *B. Am. Meteorol. Soc.*, 99, No.
714 3, 49-60, 2018.
715
- 716 Kuttippurath, J., and G. Nikulin, A comparative study of the major sudden stratospheric warmings
717 in the Arctic winters 2003/2004–2009/2010, *Atmos. Chem. Phys.*, 12, 8115–8129, 2012.
718
- 719 Livesey, N. J, M. J. Filipiak, L. Froidevaux, W. G. Read, A. Lambert, M. L. Santee, J. H. Jiang, J.
720 W. Waters, R. E. Cofield, D. T. Cuddy, W. H. Daffer, B. J. Drouin, R. A. Fuller, R. F. Jarnot,
721 Y. B. Jiang, B. W. Knosp, Q. B. Li, V. S. Perun, M. J. Schwartz, W. V. Snyder, P. C. Stek, R.
722 P. Thurstans, P. A. Wagner, H. C. Pumphrey, M. Avery, E. V. Browell, J.-P. Cammas, L. E.
723 Christensen, D. P. Edwards, L. K. Emmons, R.-S. Gao, H.-J. Jost, M. Loewenstein, J. D.
724 Lopez, P. Nédélec, G. B. Osterman, G. W. Sachse, and C. R. Webster. Validation of Aura
725 Microwave Limb Sounder O₃ and CO observations in the upper troposphere and lower
726 stratosphere. *J. Geophys. Res.*, 113:D15S02, doi: 10.1029/2007JD008805, 2008.
727
- 728 Lukianova, R., A. Kozlovsky, S. Shalimov, T. Ulich, and M. Lester, Thermal and dynamical
729 perturbations in the winter polar mesosphere-lower thermosphere region associated with
730 sudden stratospheric warmings under conditions of low solar activity, *J. Geophys. Res.*, 120,
731 5226-5240, 2015.
732
- 733 McIntyre, M. E., How well do we understand the dynamics of stratospheric warmings?, *J.*
734 *Meteorol. Soc. Japan. Ser. II*, 60, No. 1, 37-65, 1982.
735
- 736 Manney, G. L., Z. D. Lawrence, M. L. Santee, W. G. Read, N. J. Livesey, A. Lambert, L.
737 Froidevaux, H. C. Pumphrey, and M. J. Schwartz, A minor sudden stratospheric warming with
738 a major impact: Transport and polar processing in the 2014/2015 Arctic winter, *Geophys. Res.*

- 739 Lett., 42, 7808–7816, 2015.
740
- 741 Manney, G. L., M. L. Santee, L. Froidevaux, K. Hoppel, N. J. Livesey, and J. W. Waters, EOS
742 MLS observations of ozone loss in the 2004–2005 Arctic winter, *Geophys. Res. Lett.* 33,
743 L04802, doi:10.1029/2005GL024494, 2006.
744
- 745 Manney, G. L., et al., Unprecedented Arctic ozone loss in 2011, *Nature*, 478, 469–475, 2011.
746
- 747 Matsuno, T., Lagrangian motion of air parcels in the stratosphere in the presence of planetary
748 waves, *Pure Appl. Geophys.*, 118: 189–216, 1979.
749
- 750 Meraner, K., and H. Schmidt, Transport of nitrogen oxides through the winter mesopause in
751 HAMMONIA, *J. Geophys. Res. Atmos.*, 121, 2556–2570, 2016.
752
- 753 Newman, P. A., and E. R. Nash, Quantifying the wave driving of the stratosphere, *J. Geophys.*
754 *Res.*, 105, D10, 12485–12497, 2000.
755
- 756 Newman, P. A., E. R. Nash, and J. E. Rosenfield, What controls the temperature of the Arctic
757 stratosphere during the spring?, *J. Geophys. Res.*, 106(D17), 19999–20010, 2001.
758
- 759 Päivärinta, S.-M., A. Seppälä, M. E. Andersson, P. T. Verronen, L. Thölix, and E. Kyrölä ,
760 Observed effects of solar proton events and sudden stratospheric warmings on odd nitrogen
761 and ozone in the polar middle atmosphere, *J. Geophys. Res. Atmos.*, 118, 6837–6848, 2013.
762
- 763 Palmeiro, F. M., D. Barriopedro, R. Garcia-Herrera, and N. Calvo, Comparing sudden stratospheric
764 warming definitions in reanalysis data, *J. Climate*, 28, 6823–6840, 2015.
765
- 766 Pedatella, N. M., J. I. Chau, H. Schmidt, L. P. Goncharenko, C. Stölle, K. Hocke, V. L. Harvey, B.
767 Funke, and T. A. Siddiqui, How sudden stratospheric warming affects the whole atmosphere,
768 *Eos*, 99, 2018.
769
- 770 Perry, J. S., Long-wave energy processes in the 1963 sudden stratospheric warming, *J. Atmos. Sci.*,
771 24, 539–550, 1967.
772
- 773 Pommereau, J.-P. and F. Goutail, O₃ and NO₂ Ground-Based Measurements by Visible
774 Spectrometry during Arctic Winter and Spring 1988, *Geophys. Res. Lett.*, 15, 891–894, 1988.
775
- 776 Pommereau, J.-P., Goutail, F., Lefèvre, F., Pazmino, A., Adams, C., Dorokhov, V., Eriksen, P.,
777 Kivi, R., Stebel, K., Zhao, X., and van Roozendael, M.: Why unprecedented ozone loss in the
778 Arctic in 2011? Is it related to climate change?, *Atmos. Chem. Phys.*, 13, 5299–5308,
779 <https://doi.org/10.5194/acp-13-5299-2013>, 2013.
780
- 781 Rex, M., K. Dethloff, D. Handorf, A. Herber, R. Lehmann, R. Neuber, J. Notholt, A. Rinke, P. von
782 der Gathen, A. Weisheimer, and H. Gernandt, Arctic and Antarctic ozone layer observations:
783 chemical and dynamical aspects of variability and long-term changes in the polar stratosphere,
784 *Polar Research*, 19, 2, 193–203, doi: 10.1111/j.1751-8369.2000.tb00343.x, 2000.
785
- 786 Scherhag, R., Die explosionsartigen Stratosphärenenerwärmungen des Spätwinters 1951/1952,
787 *Berichte des Deutschen Wetterdienstes in der US-Zone*, 6, Nr. 38, 51–63, 1952.
788

- 789 Scheiben, D., Straub, C., Hocke, K., Forkman, P., and Kämpfer, N.: Observations of middle
790 atmospheric H₂O and O₃ during the 2010 major sudden stratospheric warming by a network of
791 microwave radiometers, *Atmos. Chem. Phys.*, 12, 7753–7765, 2012.
- 792
- 793 Schoeberl, M. R., Stratospheric warmings: Observations and theory, *Rev. Geophys.*, 16(4), 521–
794 538, 1978.
- 795
- 796 Schoeberl, M. R., and D. L. Hartmann, The Dynamics of the Stratospheric Polar Vortex and Its
797 Relation to Springtime Ozone Depletions, *Science*, 251, Issue 4989, pp. 46-52, 1991.
- 798
- 799 Seppälä, A., M. A. Clilverd, C. J. Rodger, P. T. Verronen, and E. Turunen, The effects of hard-
800 spectra solar proton events on the middle atmosphere, *J. Geophys. Res.*, 113, A11311,
801 doi:10.1029/2008JA013517, 2008.
- 802
- 803 Shepherd, M. G., S. R. Beagley, and V. I. Fomichev. Stratospheric warming influence on the
804 mesosphere/lower thermosphere as seen by the extended CMAM, *Ann. Geophys.*, 32, 589–
805 608, 2014
- 806
- 807 Smedley, A. R. D., J. S. Rimmer, D. Moore, R. Toumi, and A. R. Webb, Total ozone and surface
808 UV trends in the United Kingdom: 1979–2008, *Int. J. Climatol.* 32: 338–346, 2012.
- 809
- 810 Smit, H. G. J. and the ASOPOS panel (Assessment of Standard Operating Procedures for
811 Ozonesondes): Quality assurance and quality control for ozonesonde measurements in GAW,
812 World Meteorological Organization, GAW Report #201, Geneva, Switzerland, 2014. available
813 at: http://www.wmo.int/pages/prog/arep/gaw/documents/FINAL_GAW_201_Oct_2014.pdf.
- 814
- 815 Smith-Johnsen, C., Y. Orsolini, F. Stordal, V. Limpasuvan, and K. Pérot, Nighttime mesospheric
816 ozone enhancements during the 2002 southern hemisphere major stratospheric warming, *J.*
817 *Atmos. Sol-Terr. Phys.*, 168, 100-108, 2018.
- 818
- 819 Solomon, S., Stratospheric ozone depletion: A review of concepts and history, *Rev. Geophys.*, 37,
820 275-316, 1999.
- 821
- 822 Solomonov, S. V., E. P. Kropotkina, S. B. Rozanov, N. A. Ignat'ev, and A. N. Lukin, Influence of
823 strong sudden stratospheric warmings on ozone in the middle stratosphere according to
824 millimetre wave observations, *Geomag. Aeron.*, 57, 3, 361-368, 2017.
- 825
- 826 Sofieva, V. F., N. Kalakoski, P. T. Verronen, S.-M. Päivärinta, E. Kyrölä, L. Backman, and J.
827 Tamminen, Polar-night O₃, NO₂ and NO₃ distributions during sudden stratospheric warmings
828 in 2003–2008 as seen by GOMOS/Envisat, *Atmos. Chem. Phys.*, 12, 1051-1066, 2012
- 829
- 830 Strahan, S. E., A. R. Douglass, and S. D. Steenrod, Chemical and dynamical impacts of
831 stratospheric sudden warmings on Arctic ozone variability, *J. Geophys. Res.*, 121, 11836-
832 11851, 2016.
- 833
- 834 Tao, M., P. Konopka, F. Ploeger, J.-U. Groöf, R. Muller, C. M. Volk, K. A. Walker, and M. Riese,
835 Impact of the 2009 major sudden stratospheric warming on the composition of the stratosphere,
836 *Atmos. Chem. Phys.*, 15, 8695-8715, 2015.
- 837
- 838 Tegtmeier, S., M. Rex, I. Wohltmann, and K. Krüger, Relative importance of dynamical and

- 839 chemical contributions to Arctic wintertime ozone, *Geophys. Res. Lett.*, 35, L17801, 2008a.
840
- 841 Tegtmeier, S., K. Krüger, I. Wohltmann, K. Schoellhammer, and M. Rex, Variations of the residual
842 circulation in the Northern Hemispheric winter, *J. Geophys. Res.*, 113, D16109,
843 doi:10.1029/2007JD009518, 2008b.
844
- 845 Trenberth, K. E., Dynamic coupling of the stratosphere with the troposphere during sudden
846 stratospheric warmings, *Monthly Weather Review*, 101, 4, 306-322, 1973.
847
- 848 Tripathi, O. P., et al., The predictability of the extratropical stratosphere on monthly time-scales
849 and its impact on the skill of tropospheric forecasts, *Q. J. R. Meteorol. Soc.*, 141, 987-1003,
850 2015.
851
- 852 Vandaele, A. C., Fayt, C., Hendrick, F., Hermans, C., Humbled, F., Van Roozendael, M., Gil, M.,
853 Navarro, M., Puentedura, O., Yela, M., Braathen, G., Stebel, K., Tornkvist, K., Johnston, P.,
854 Kreher, K., Goutail, F., Mieville, A., Pommereau, J.-P., Khaykin, S., Richter, A., Oetjen, H.,
855 Wittrock, F., Bugarski, S., Friez, U., Pfeilsticker, K., Sinreich, R., Wagner, T., and Corlett, G.,
856 and Leigh, R.: An intercomparison campaign of ground-based UV-visible measurements of
857 NO₂, Br_o, and OClO slant columns: Methods of analysis and results for NO₂, *J. Geophys.*
858 *Res.*, 110, D08305, doi:10.1029/2004JD005423, 2005.
859
- 860 Vaughan, G., Roscoe, H., Bartlett, L. M., O'Connor, F. M., Sarkissian, A., Van Roozendael, M.,
861 Lambert, J.-C., Simon, P., Karlsen, K., Kastad Hoiskar, A., Fish, D., Jones, R., Freshwater, R.,
862 Pommereau, J.-P., Goutail, F., Andersen, S., Drew, D., Hughes, P., Moore, D., Mellqvist, J.,
863 Hegels, E., Klupfel, T., Erle, F., Pfeilsticker, K., and Platt, U.: An intercomparison of ground-
864 based UV-visible sensors of ozone and NO₂, *J. Geophys. Res.*, 102, 542–552, 1997.
865
- 866 Waters, J. W., W. G. Read, L. Froidevaux, R. F. Jarnot, R. E. Cofield, D. A. Flower, G. K. Lau, H.
867 M. Pickett, M. L. Santee, D. L. Wu, M. A. Boyles, J. R. Burke, R. R. Lay, M. S. Loo, N. J.
868 Livesey, T. A. Lungu, G. L. Manney, L. L. Nakamura, V. S. Perun, B. P. Ridenoure, Z.
869 Shippony, P. H. Siegel, R. P. Thurstans, R. S. Harwood, H. C. Pumphrey, and M. J. Filipiak,
870 The UARS and EOS Microwave Limb Sounder (MLS) Experiment, *J. Atmos. Sci.*, 56, 194-
871 218, 1999.
872
- 873 Yamazaki, Y., M. J. Kosch, and J. T. Emmert, Evidence for stratospheric sudden warming effects
874 on the upper thermosphere derived from satellite orbital decay data during 1967–2013,
875 *Geophys. Res. Lett.*, 42, 6180–6188, 2015.
876
877